J Nanopart Res (2013) 15:2095
DOI 10.1007/s11051-013-2095-2

RESEARCH PAPER

Percolation network dynamicity and sheet dynamics governed viscous behavior of polydispersed graphene nanosheet suspensions

Purbarun Dhar · Mohammad Hasan Dad Ansari · Soujit Sen Gupta · V. Manoj Siva · T. Pradeep · Arvind Pattamatta · Sarit K. Das

Received: 9 August 2013 / Accepted: 22 October 2013 / Published online: 7 November 2013

Abstract The viscosity of polydispersed graphene nanosheet (5 nm–1.5 μm) suspensions (GNS) and its behavior with temperature and concentration have been experimentally determined. A physical mechanism for the enhanced viscosity over the base fluids has been proposed for the polydispersed GNSs. Experimental data reveal that enhancement of viscosity for GNSs lies in between those of carbon nanotube suspensions (CNTSs) and nano-alumina suspensions, indicating the hybrid mechanism of percolation (like CNTs) and Brownian motion-assisted sheet dynamics (like alumina particles). Sheet dynamics and percolation, along with a proposed percolation network dynamicity factor, have been used to determine a dimensionally consistent analytic model to accurately determine and explain the viscosity of polydispersed GNSs. The model also provides insight into the mechanisms of viscous behavior of different dilute nanoparticle suspensions. The model has been found to be in agreement with the GNS experimental data, and even for CNT (diameter 20 nm, length 10 μm) and nano-alumina (45 nm) suspensions.

Keywords Graphene · CNT · Alumina · Nanofluid · Nanoparticle · Viscosity · Percolation · Particle dynamics · Modeling and simulation

Purbarun Dhar and Mohammad Hasan Dad Ansari have contributed equally to this study.

P. Dhar · V. M. Siva · A. Pattamatta · S. K. Das (✉)
Department of Mechanical Engineering, Indian Institute of Technology Madras, Chennai 600036, India
e-mail: skdas@iitm.ac.in

M. H. D. Ansari
Department of Mechanical Engineering, Indian Institute of Technology Patna, Patna 800013, India

S. S. Gupta · T. Pradeep
Department of Chemistry, Indian Institute of Technology Madras, Chennai 600036, India

Introduction

Graphene, the two-dimensional (2D) allotrope of carbon, has revolutionized scientific research in the recent years. Graphene being a collective ensemble of unique properties (Geim and Novoselov 2007), it is also important to study graphene when dispersed as micro or nanosheets in a fluid medium. Since the inception of research in nanosuspensions or nanofluids (dilute suspensions of nanoparticles in a suitable base fluid), the academic community world over has studied their thermal properties in great detail. However, in-depth research into other physical properties has remained scarce as yet. One such property is the viscosity of nanosuspensions and its implications in consequent applications. Graphene nanosuspensions (GNSs) may soon emerge as the raw materials for graphene-based thin films and printed electronic devices, as fluids with tunable electric and/or thermal

conductivities or as bio-nanosuspensions for targeted drug delivery. All such applications require motion of graphene sheets within the fluid or of the bulk suspension itself. Thus, the innate need to understand the viscosity of GNSs is of prime importance for development of the aforementioned technologies. In this article, we experimentally study the viscosity of GNSs and propose a mechanism for the enhancement of viscosity over the base fluid and the viscous behavior of the polydispersed GNSs.

Studies on the viscosity of dispersed systems can be traced back to Einstein's model (Einstein 1906), which expressed the viscosity of the suspension as a simple linear function of the viscosity of the base fluid and the volume fraction of particle loading. However, the model has been found to be consistent with experimental data only at vanishingly low concentrations of spherical particles. Moreover, the model does not incorporate the effects of particle size on the viscosity of the system. Over the years, many modifications were brought about by numerous researchers onto Einstein's classical model. Some of the more famous models in this genre are those by Bachelor (1977), Krieger and Dougherty (1959), Eilers and Die (1941), de Bruijn (1942), Pak and Cho (1998), and Wang and Mujumdar (2007). Majority of these models incorporated the effects of particle migration based on Brownian motion and added an effective higher power term of particle concentration to the existing linear model by Einstein. However, the success of the models remained confined to very low volume fractions. Also, the viscosity remained independent of the size effects, and temperature effects on viscosity could not be explained by these models. The change in the viscosity of the base fluid with temperature is the only temperature-dependent term in all such models.

It is also of prime importance to understand the viscous behaviors of nanosuspensions of CNT and ceramics like alumina, since many important behaviors of novel materials like CNT-based self-cleaning surfaces (Sethi et al. 2008) or alumina-based micropatterning masks (Banerjee et al. 2013) depend on the viscosity of the nanosuspensions, which are often the raw materials to manufacture such devices. Several other models for the viscosity of dispersed systems have been proposed based on several mechanisms, viz. Kinetic Theory (Kulkarni et al. 2006) (viscosity expressed as an exponential function of temperature), Interparticle spacing (Graham 1981), Liquid layering (Avsec and Oblak 2007) (viscosity expressed as high-order polynomial of volume fraction), particle mean free path (Chandrasekar et al. 2010; Tseng and Lin 2000), Brownian diffusion of particles (Murshed et al. 2008; Masoumi et al. 2009), etc. Many of such models are purely empirical in nature, lack dimensional consistency, and cannot provide clear insight into the actual physical mechanism behind increase in viscosity or the viscous behavior. Furthermore, many of the models work accurately only for specific shapes and types of dispersed media and do not take into account property variations of the dispersed system. Several experimental reports on viscosity of nanofluids have been published over the last decade. Nguyen et al. (2007) reported experimental viscosity data for Al_2O_3–water and CuO–water and provided completely empirical correlations for the viscosity of the nanofluids. Anoop et al. (2009) looked into the electroviscous effects in pH-stabilized nanofluids and proposed a mechanism to explain the effects of particle agglomeration and effect of the Debye–Huckel screening length on the stability and viscosity of nanofluids. He et al. (2007) reported experimental observations for TiO_2 nanoparticle suspensions; however, no physical explanation for the viscous behavior was provided, while Namburu et al. (2007) reported Newtonian behavior for CuO nanoparticles in 60:40 ethylene glycol and water mixture with only a deduced empirical model for nanofluid viscosity. Likewise, only experimental data and empirical correlations were provided by Kole and Dey (2010) for alumina-engine oil nanofluids. Viscous behaviors of Chitosan stabilized Multi Wall CNT nanosuspensions were reported by Phuoc et al. (2011); however, the report lacked any physical explanations for the observations. Implications of nanofluid viscosity for thermal applications were experimentally determined by Prasher et al. (2006) and Murshed et al. (2008), but no physical mechanism for the viscous behaviors of nanofluids was provided. Also to be noted, in most of the cases discussed above, the nanosuspensions utilized were of typically high concentrations (>2 vol%). This leads to particle overcrowding within the fluid matrix, and various other governing mechanisms creep into the system, and hence, it is recommended to study dilute systems (<1 vol%) to develop the clear picture. As for the present case, a proper understanding of the underlying physics that governs GNS viscosity (detailed studies on the subject matter have been very

rare) is needed for prolonged technical advancements in the field.

Methods

Nanosuspensions: preparation and characterization

Preparation of graphene involves a two-step process (Dreyer et al. 2010): oxidation of graphite power to graphite oxide (GO) based on modified Hummer's process (Li et al. 2008), followed by reduction of GO to Reduced GO (RGO). First, 1 g of Graphite powder (procured from R. K. Scientific Pvt. Ltd.) was taken and 12 mL of concentrated H_2SO_4 was added, and the mixture was allowed to stand at 90 °C for an hour. Tothis mixture, 2 g of $K_2S_2O_8$ and P_2O_5 each was added with constant stirring and kept for 6 h at the same temperature for preoxidation of Graphite. The mixture was then cooled to room temperature and filtered. The filtrate was discarded, and the preoxidized GO was kept for drying in hot air oven overnight. To the dry preoxidized GO, 24 mL of concentrated H_2SO_4 was added and kept at ice-cold condition. Then, 3 g of $KMnO_4$ was added slowly under constant stirring. The mixture was allowed to stand for 6 h under stirring condition. Then 400 mL of distilled water was added slowly under stirring condition and kept at room temperature for an hour. The reaction was stopped after adding 5 mL of 20 % H_2O_2, and the mixture was kept undisturbed overnight. A bright yellow-colored precipitate confirmed the conversion to GO. The solution was decanted, and the precipitate was washed with 1 % HCl thrice. This solution was centrifuged to collect GO. The GO was dried in vacuum for 24 h. After drying, 1 g of GO was weighed and redispersed in deionized water such that the concentration of the GO solution was 0.5 wt%. This solution was further dialyzed to remove the unwanted ions. This GO solution was kept as the stock solution for the preparation of graphene. From this, 100 mL of GO solution was taken, and 200 mg of $NaBH_4$ was added and kept under stirring for about an hour for reduction of the functional groups present. The solution was filtered and prereduced graphene was separated, and then, 100 mL of water was added. This was further sulfonated with sulfanilic acid to make graphene nanosheet suspensions dissolved in water as the base medium. The 0.5 wt% RGO solution prepared was kept as the stock solution. This solution was diluted with water for getting other RGO nanofluids of lower concentrations.

The prepared graphene was characterized by analyzing its Raman spectrum. The characteristic peaks of graphene at 1,348 and 1,598 cm^{-1} represent the D and G bands, respectively (shown in Fig. 1a). The D band represents the defects, and the G band represents the in-plane stretching of sp2 carbon in graphene. The presence of 2D band at around 2,800 cm^{-1} confirms the existence of graphene. The ratio of I2D/IG is in the range of 0.34–0.5, which indicates that the graphene utilized in the present study is bi and/or trilayered (Kurra et al. 2013). Transmission electron microscopy

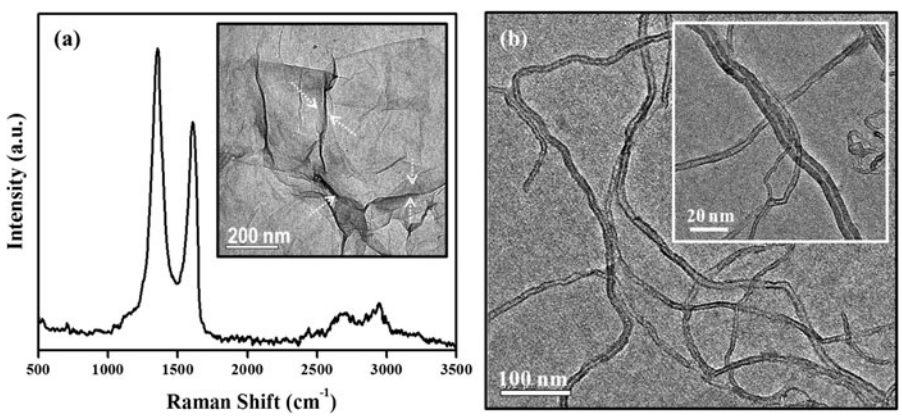

Fig. 1 **a** Raman spectrum of graphene. *Inset* (**a**): TEM image of graphene (wrinkles in graphene sheets have been marked with *arrows*). **b** TEM image of CNTS. *Inset* (**b**) evidence of percolation network formation in CNT

(TEM) was carried out for further characterization of the graphene sheets (Fig. 1a).

Nano alumina suspensions (nAS) and carbon nanotube suspensions (CNTS) were also prepared to observe their viscous behaviors for the purpose of comparison. The method to prepare nAS involves dispersing alumina nanoparticles as dry powder in base fluids and stabilizing the system. Alumina nanoparticles (particles in the size range of 40–50 nm) were procured from the commercial manufacturer Alfa Aeser, USA. Required amounts of alumina were weighed and dispersed in DI–water samples without the use of any surfactants. Ultrasonication for 1 h was needed to stabilize the nanofluids. The shelf-life stability for such nAS was found to exceed a month.

The CNTSs were similarly prepared. The required amount of dry CNT (procured from NaBond Technologies, China) was weighed and mixed in DI water samples to get the required concentrations. Sodium dodecyl sulfate (SDS) was used as surfactant, and the CNTSs were ultrasonicated for an hour. The SDS-stabilized CNTSs were found to have shelf-life stability over 6 months. The TEM image of the CNTS (Fig. 1b) reveals the presence percolation networks.

Experimental and measurement details

The fluid viscosities for different loading concentrations and temperatures have been determined using an automated microviscometer (Anton Paar GmbH, Austria). It is a rolling-ball viscometer which works in accordance with the principle of a falling ball within a fluid media. A stainless-steel ball descends through a closed, liquid-filled capillary which is inclined at a defined angle. Inductive sensors determine the ball's time of descent. Both the dynamic and kinematic viscosities of the liquid can be calculated from the rolling time. In the present study, a capillary of internal diameter of 1.6 mm and a steel ball of diameter 1.5 mm have been used. An in-built heating element and a precision Peltier thermostat allow performing measurements at different temperatures. The angle of tilt for the capillary was set to 30° so as to allow at least 10-s descent time for all the measurements (to prevent formation of any turbulence within the capillary). Ten viscosity readings were taken for each temperature, and their average was taken as the final value. The deviation among each dataset was found to be within ±3 %.

Results and discussion

Experimental observations

The effects of temperature on the viscosity of dilute nanosuspensions were experimentally investigated. Low concentrations were studied so as to reveal the exact mechanism of enhancement in viscosity without factors like particle agglomeration, particle crowding, and sedimentation creeping into the forefront. The viscosity of the nanosuspensions has been found to increase with concentration and decrease with temperature. However, different particles have been seen to behave very differently in the fluid medium. While, in the case of nAS, the effect of concentration (within dilute limits) on the viscosity of the suspension is negligible, the response shown by the CNTSs to concentration is highly pronounced. Interestingly enough, the trend shown by the GNSs lies nearly midway between the nAS and the CNTSs. The trends in nanofluid viscosity with concentrations at 298 K have been provided in Fig. 2a. This trend in GNSs behavior has also been seen in the case of GNSs thermal conductivity (Gupta et al. 2011). From such behavior, it can be hypothesized that the mechanism of viscosity enhancement in GNSs is also a hybrid of the mechanisms for nAS and CNTSs. Furthermore, as seen in Fig. 2b, the ratio of the viscosity of the suspension to the viscosity of the base fluid shows an inverted bell-shaped trend for CNTS and a perfectly flat trend for nAFs. The trend in the case of GNS can be seen to be a somewhat flattened inverted bell, which again brings to the forefront the possibility of the existence of dual mechanism of viscous behavior in the case of the GNSs.

Mathematical modeling

The mathematical model has been formulated considering an elemental cubic cell within the nanosuspensions as the analytic domain. The dimension of the domain is evaluated on the basis of percolation theory for GNSs (Dhar et al. 2013). The mechanism behind the viscous behavior of the GNSs can be explained by considering the GNS to be a polydispersed system, where the behavioral aspects of any individual graphene sheet are dependent on the critical sheet size (CSS) (Dhar et al. 2013) of graphene sheets for the system. The CSS theory states that for each dispersed media-

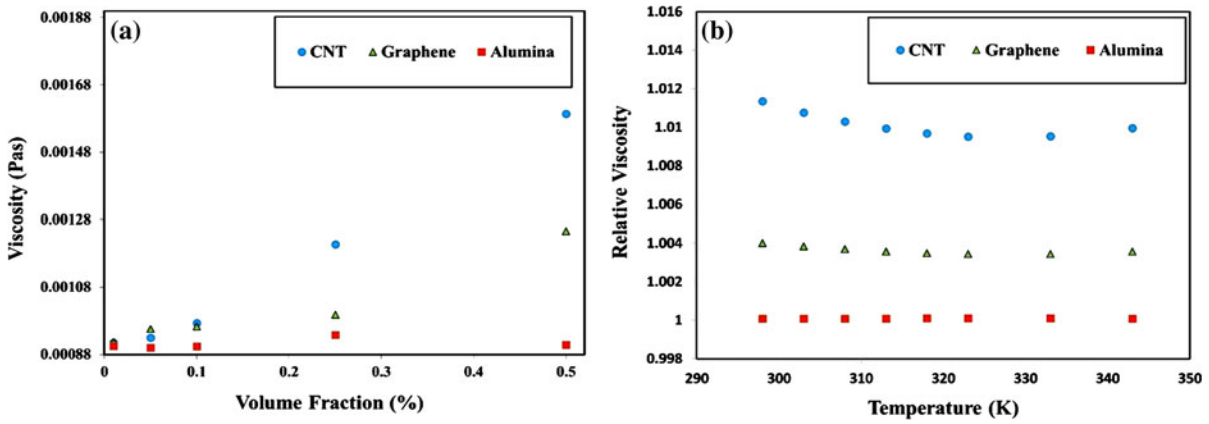

Fig. 2 **a** Response of suspension viscosity to particle concentration at constant temperature (298 K). **b** Suspension viscosity/base fluid viscosity response against temperature for 0.01 vol% conc

base fluid pair; there exists a critical particle or sheet size that determines particle behavior within the suspension. Particles of sizes larger than this will show tendency to percolate into networks, and those smaller than the critical size are dominated by the Brownian randomness within the medium. Based on this critical size, the graphene sheets can be categorized into two types, viz. micronscale sheets, which promote viscosity by forming percolation networks, and nanoscale sheets, which promote viscosity due to their Brownian motion-induced randomness. In essence, the formulation for the viscosity induced by sheet percolation is similar to that of Einstein's formulation; however, the present model is able to explain the viscous effects due to the size of the sheets, the concentration, as well as the configuration of the percolation network with temperature. The viscosity due to sheet dynamics has been derived based on dimensional analysis, and the present approach provides insight into the micro-nano-scale dispersed phase–fluid interactions that govern the viscosity of nanosuspensions.

The expression for the viscosity of GNSs induced by sheet percolation is theorized as

$$\mu_{\text{perc}} = \mu_{\text{bf}}(1 + L^* d\phi\alpha), \tag{1}$$

where μ_{perc} is the viscosity of the GNS induced by the percolation networks, μ_{bf} is the viscosity of the base fluid at the temperature at which the viscosity of the nanosuspensions needs to be determined, L* is the nondimensionalized length scale and is the ratio of the average graphene sheet face length to the CSS at that temperature ($L^* = L_G/L_{\text{crit}}$, where L_G is the average sheet face size for graphene sample and L_{crit} is the CSS for the graphene–base fluid pair), d is the percolation network dynamicity factor (NDF), φ is the loading fraction (concentration) of nanoparticles, and α is the sheet distribution fraction (Dhar et al. 2013). The expression has been derived along the lines of Einstein's model[2] for viscosity of very dilute suspensions. However, it has been proposed that the viscosity of the nanosuspensions is related to the volume fraction of loading by a temperature-dependent factor termed the percolation NDF. Within GNSs, the relative motion between adjacent fluid layers or between the fluid and a foreign object is hampered by the presence of the long percolation networks. It has been hypothesized that although the sheets forming these percolation networks are too massive to be affected appreciably by Brownian motion, they undergo constant rearrangements within the network itself (without compromising the integrity of network as a whole), due to the constant bombardment by the smaller Brownian-dominated sheets and due to the vibrations of neighboring fluid molecules.

Unlike thermal conductivity, where the mechanism is dependent on the length of the percolation paths (Dhar et al. 2013), viscosity of the GNS is affected by the reshufflings occurring within the networks. This is because viscosity of the fluid is sensitive to any relative motion with respect to the fluid molecules. The reshufflings lead to competitive interplay in between the cohesive forces between the neighboring sheets and the adhesion between the sheets and fluid molecules. The constant interplay between the two forces leads to changes in the magnitude of the

induced viscosity at the molecular level. Furthermore, fluidic interlayer shear within the domain is higher in the presence of a dynamic body than a static body. As a result, the dynamic, reshuffling sheets within the networks lead to more induced viscosity than static sheets. Since the Brownian velocity of the smaller sheets and the vibrational energy of the fluid molecules increase with temperature, the NDF also changes. The magnitude of the NDF provides a qualitative estimate of the overall degree of dynamicity within the networks. A smaller value of the NDF implies less reshuffling within the network and hence more stability of the network.

While mathematically modeling the viscous behavior due to the presence of percolating micro-nanostructures within the fluid, the trend exhibited by the relative viscosity (ratio of viscosity of nanosuspension to the viscosity of base fluid) needs to be invoked. It is observed from experimental data analysis that the presence of percolating micronanostructures introduces nonlinearity to the relative viscosity data with respect to temperature. In order to determine the magnitude of the proposed NDF, it becomes necessary to map the nonlinearity in terms of a suitable polynomial function. To achieve this, it has been assumed that the NDF behavior with temperature for any nanosuspension exhibiting percolation structures can be accurately approximated using a proper quadratic function. Its behavior with temperature has been expressed in Eq. (2)

$$d = A^*T^2 + B^*T + C^* \tag{2}$$

The parameters A^*, B^*, and C^* are the coefficients for such a quadratic function and are determined from the experimental data (Fig. 2b). The analytic model derived for explaining and predicting the viscosity of nanosuspensions is based on certain physically consistent and valid assumptions. Consequently, the predicted values of viscosity from theory are not exact but of the order of magnitude of the exact values. It is only by mapping a polynomial function to mimic the trend of relative viscosity that the near-exact solutions can be achieved. A^*, B^*, and C^* are nonadjustable constants for a particular solute–solvent pair. For graphene–water pair, the values of A^*, B^*, and C^* are deduced to be approximately 0.75, $-463.5\ K^{-1}$, and 71,682, respectively, and the values have been found to be highly consistent for all volume fractions. The seemingly odd quadratic behavior of the NDF in respect of absolute temperature (Fig. 3d) can be explained based on the philosophy of multiple body interactions. Qualitative illustrations have been

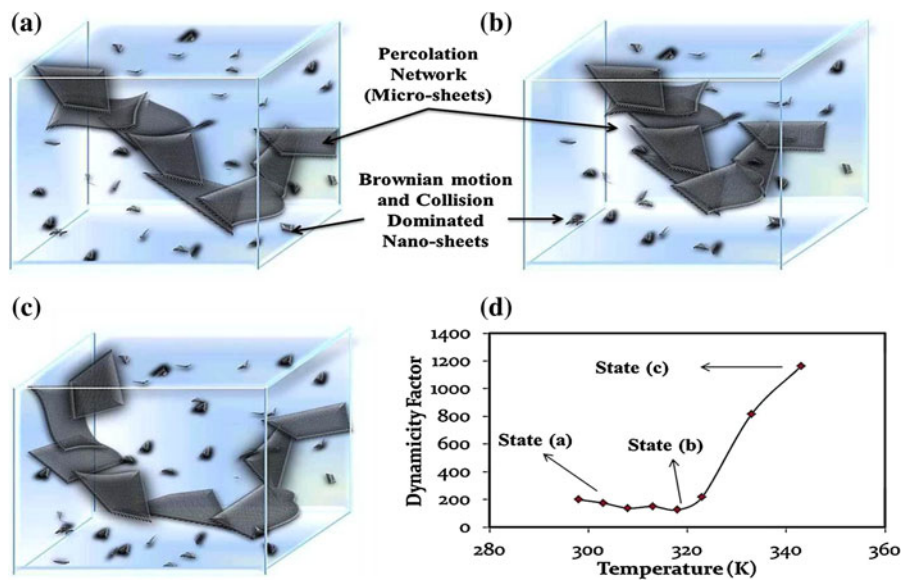

Fig. 3 NDF behavior for GNS with temperature. Network configurations at **a** 300 K, **b** 320 K, **c** 333 K, and **d** the trend of the term ($L^* \times d$) with temperature. The graphic configuration details for the hypothesis at different temperatures provided are purely qualitative in nature

provided in Fig. 3a–c for establishing the NDF hypothesis. A system composed of multiple similar components, when agitated from its initial state (Fig. 3a) with small agitations, will slowly begin to assemble toward a more composed state (Fig. 3b), i.e., a state of the least total energy. However, after this, if the agitations are continued with larger agitation amplitude, then the state of the least energy collapses, and the system starts to deviate toward its original state, and with the increasing amplitudes, the randomness keeps increasing out of proportion (Fig. 3c). An example of such a system would be some sand on a tray. When the tray is slowly shaken, the sand particles will tend to collect toward one region of the tray, creating a state of minimum randomness. However, when the shaking force increases and becomes aggressive, the sand particles scatter out in all directions, increasing the randomness largely.

In the case of percolation networks within GNS, temperature-induced Brownian motion of the smaller sheets and the vibration of the liquid molecules act as the sources of agitations. As temperature increases, the initial configurations are reshuffled and tend to make the network compact, as suggested by the decreasing NDF. However, as temperature becomes higher, the agitation increases, causing the frequency of reshuffling to increase. This leads to increased values of the NDF. Given the micronscale size of percolating graphene sheets (nearly equal to the CSS), the dynamicity induced becomes very high at higher temperatures. As evident from Fig. 2b, the NDF has a direct relationship to the induced viscosity. As the system attains static configurations, the relative viscosity value decreases, whereas, with increasing dynamicity, the relative viscosity also increases.

At first glance, the viscosity due to percolation networks seems independent of the size of individual sheets. However, the model is not completely independent of the sheet length scales. The factor L^* governs the viscous behavior of the GNS. For values of L^* below unity, the viscosity rendered by percolation disappears because percolation does not take place in such conditions. As the value of L^* grows, the viscous effects rendered multiplies alongside it. This observation too can be considered as a direct consequence of interplay between the forces of cohesion and adhesion. Sheets of larger sizes are in contact with more fluid molecules than smaller sheets. The surfaces in contact between neighboring sheets are also higher than smaller sheets. This leads to higher cohesion–adhesion interactions and the perturbations induced at the molecular level due to interplay of the forces are higher. As a result, the viscous effects are higher for larger percolating bodies. It has been hypothesized that the viscosity due to percolation is a simple direct product of L^* and the NDF.

The viscosity rendered to the GNS by sheet dynamics has been hypothesized to be qualitatively analogous to the behavior of gas molecules and has been derived from the dimensional analysis. A gas can be structurally viewed as a collection of individual molecules within a matrix of free space (vacuum). The molecules, owing to their thermal energy, randomly move about in space, colliding with neighboring molecules in the process. In a nanosuspension, each nanoparticle traverses within the fluid matrix (Brownian motion) due to the thermal energy possessed by the particle, and in the process, collides with neighboring particles. This behavior can be treated analogous to the gas molecules, wherein, the fluid matrix behaves qualitatively as the vacuum-free space in the case of the gas molecules. Since it is important to model the mean free path of particle collisions on the viscous behavior, a gas-like model has been introduced (mean free path being an important concept to explain gaseous behavior).

The equation for the viscosity due to sheet dynamics is expressed in Eq. (3):

$$\mu_{\mathrm{sd}} = \mu_0 \phi (1 - \alpha), \tag{3}$$

where μ_{sd} is the viscosity induced by sheet dynamics. The variable "μ_0" is the dynamic viscosity term and can be expanded as

$$\mu_0 = \rho_{\mathrm{G}} \lambda U_{\mathrm{B}} \theta, \tag{4}$$

where ρ_{G} is the density of graphene, λ is the mean free path of intersheet collisions, U_{B} is the Brownian velocity of the sheets as given by Stokes–Einstein's formula as given in Eq. (5) (k_{B} is the Boltzmann constant, T is the absolute temperature, L_{G} is the average face size of the dynamic graphene nanosheets), and θ is the collision cross section.

$$U_{\mathrm{B}} = \frac{2 k_{\mathrm{B}} T}{\pi \mu_{\mathrm{bf}} L_{\mathrm{G}}^2} \tag{5}$$

The viscosity of the GNS due to sheet dynamics is directly proportional to the density of the dispersed media. For two particles of different densities, the

particle with higher density is more massive, and upon being set into random motion by the thermal disturbance of the fluid molecules, experiences higher inertial drag and relaxation within the fluid than a particle of lower density, which travels more freely through the fluid. The combined retarding forces induce higher shear between the particle–fluid molecule interfaces, and leads to enhanced viscosity. Therefore, a denser suspended media renders higher viscous resistance in between adjacent fluid layers than a lower density media. However, it is noteworthy that if the density of the particle is too high, so as to induce sedimentation, then the viscous behavior might be completely different.

As evident from Eq. (4), the system will have higher induced viscosity if the mean free path of interparticle collisions is higher. The mean free path for nanoparticles suspended in a fluid medium has been hypothesized to be of the order of a few microns at 298 K. The behavior of the mean free path can be expressed as $\lambda = (L \times 10^{-6})$ meter, where "L" is a temperature-dependent variant. Since it is difficult to ascertain the theoretical value of "L" for each temperature value, the product of "$L\theta$" can be utilized [as expressed in Eq. (6)] for the ease of mathematical manipulation. The equation [Eq. (6)] has been proposed along the lines of the assumption that the nanosheets behave analogous to gas molecules, and hence, their mean free path of collision has been analogously considered as an exponentially decaying function of absolute temperature. A larger mean free path physically signifies the low frequency of interparticle collisions and thereby more travel time for the nanosheets between subsequent collisions. Large values of travel time lead to increased sheet–fluid molecule interactions and thereby prolonged time-scales for shear to develop and exist between the two components. In a system with a lower mean free path (for the same volume concentration and temperature), the time-scale of such molecular shear is essentially reduced, and thus the viscosity induced within the system is reduced.

$$L\theta = Be^{-CT} \tag{6}$$

The viscosity is also high for larger values of Brownian velocity. While this might sound contradictory to the explanation for the mean free path, it is physically consistent. A higher value of Brownian velocity (signifying more collisions and hence less induced viscosity as per the explanation for mean free path) induces higher amounts of microscale eddies within the fluid matrix. The presence of such eddies leads to drastically increased viscosity of the system. The collision cross section gives an idea into the probable number of intersheet collisions taking place within the domain at a given instant of time. With the increasing number of collisions in a frozen time frame, the viscosity of the system increases. This is because the increasing number of collisions in a frozen instant of time leads to generation of more microscale eddies and localized microvortices within the system, thereby increasing the system's effective viscosity. The collision cross section is deduced from experimental data to be a linear function of temperature and can be expressed as $\theta = (aT - b)$ (Dhar et al. 2013), where "a" and "b" are constants.

From the above discussion, it can be concluded that unlike the viscosity rendered by sheet percolation, which can be completely eliminated by utilizing graphene sample of sheet sizes below the CSS, the viscosity rendered by sheet dynamics becomes difficult to reduce. While, at lower temperatures, the induced viscosity is high due to large mean free paths, at higher temperatures, it still remains appreciably high due to increased Brownian velocity and consequent microeddy and/or microvortices formation. As a result, the relative viscosity almost remains constant across a wide temperature range. Considering all these factors, the effective viscosity of the GNS is theorized to be the summation of the two contributing viscosities and can be expressed as

$$\mu_{\mathrm{GNS}} = \mu_{\mathrm{perc}} + \mu_{\mathrm{sd}}. \tag{7}$$

The viscosity of GNSs with volume concentration and temperature are seen in Figs. 4 and 5, respectively. In the present study, the average graphene sheet size larger than the CSS is approximately 1.5 microns (from DLS analysis), and so the value of L^* is approximately 1.25. For graphene–water pair, the values of "B" and "C" are determined to be 6.95×10^6 and 0.0327, respectively. The values of "a" and "b" are found to be 50 and 15,100, respectively (for $T \geq 303$ K), and 1.66 and 454, respectively (for $T < 303$ K). In the case of water as base fluid, it is observed that the number of collisions at any instant increases at a much higher rate greater than 303 K. This phenomenon has been found to be consistent even for nASs.

It is seen from Figs. 4 and 5 that the model slowly deviates from the experimental values as the concentration reaches 0.5 vol%. This is because around and greater than this loading, several other factors begin to disrupt the mechanisms of network dynamicity and sheet dynamics that govern the present model. The present model has been deduced based on the assumption that the concentration is low enough to allow free dynamicity of the percolation structures and uninhibited dynamic nature of the nanosheets. The free rearrangements and dynamicity of the networks and the sheets, respectively, are hampered by excessive sheet crowding (high population density of sheets within the fluid matrix) due to high concentrations. Consequently, nonlinear modes of viscous behavior are induced within the system, making the theoretical predictions lesser in magnitude than the experimental values. Interestingly for GNS, in such a scenario, analysis yields that the simple percolation term of the composite viscosity model can predict the viscosity at low temperatures (Fig. 5). This is evidence for excessive static behavior among the nanosheets due to sheet crowding, arising due to the increased cohesion–adhesion interplay due to the increased number of particles within the system. However, as temperatures rise, dynamicity is gained by both the networks and the nanosheets to some extent, and the composite model can predict the viscosity at high temperatures. This behavior evidences that the present explanation is physically consistent.

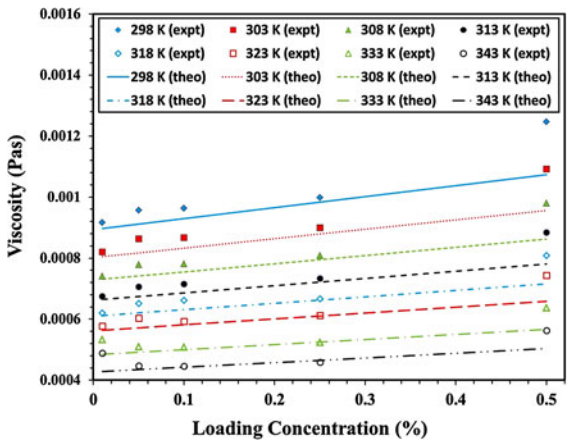

Fig. 4 Validation of analytic model for GNS with experimental data for different loading concentrations

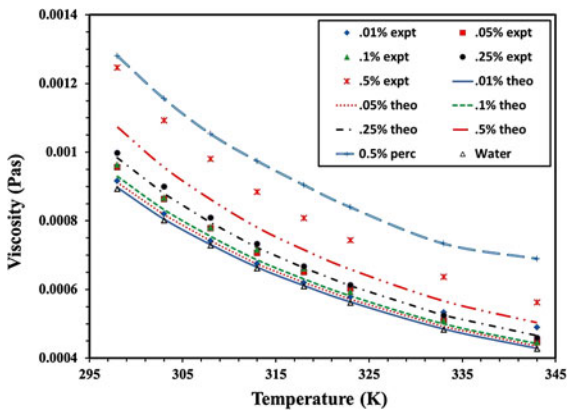

Fig. 5 Validation of analytic model for GNS with experimental data for different temperatures

The composite model for GNSs has been validated both for a completely percolating system and a completely dynamic system. For a purely percolating system, CNT–water suspension has been used, while nAS is used for studying purely dynamic systems. For a purely percolating system, i.e., CNTS, "α" is unity, and the expression for viscosity reduces to

$$\mu_{\mathrm{CNTS}} = \mu_{\mathrm{bf}}(1 + L^{*}d\phi). \tag{8}$$

In the case of CNTS, the fluid matrix is composed solely of dispersed CNT, forming dense percolation networks. The plots for viscosity of CNTSs with concentration and temperature are seen in Figs. 6 and 7, respectively. In the present study, the CNT used has a diameter of 20 nm and a length of 10 microns on an average, making the L^{*} value approximately 10. The values of A^{*}, B^{*}, and C^{*} for CNT–water pair are determined to be 0.0021, -1.377, and 235 K^{-1}, respectively. As explained earlier, from around 0.5 vol%, the viscosity begins to diverge away from the predicted values. In experimental setups where the viscosity is measured by the falling ball principle within a capillary, this phenomenon is enhanced as overcrowded networks within a confined capillary provide higher viscous resistance. Technically, CNTs, with their large aspect ratios, form stronger networks which are more resilient to temperature but exhibit much higher perturbations due to the increased adhesion–cohesion interplay, inducing more viscosity than GNSs. This fact is verified from the NDF behaviors of the two forms of carbon. While CNT networks are less disturbed by temperature effects and the viscosity is more governed by molecular perturbations due to adhesion–cohesion interactions, the NDF of graphene sheets are very high, implying high

degrees of readjustment and reshuffling among the members within the networks. However, due to the ability of CNTs to form very long networks, the induced viscosity is higher than GNSs for the same volume fraction and temperature.

As evident from Figs. 6 and 7, CNTS exhibits higher degrees of deviation from the proposed theory for dilute nanosuspensions than GNS. Such a phenomenon can be explained based on the high aspect ratio of CNT. At concentrations deviating away from the dilute limits, the network structure formed by CNT members becomes highly packed and dense, and owing to the large aspect ratio, leads to a system mimicking a 3D wire-mesh. As a consequence, dynamicity of the network is highly arrested, and adhesion–cohesion interplay dominates, making the viscous behavior nonlinear in nature. The proposed model, being derived for the dilute domain, does not map the nonlinearity effects and thus falls short of predicting the actual value.

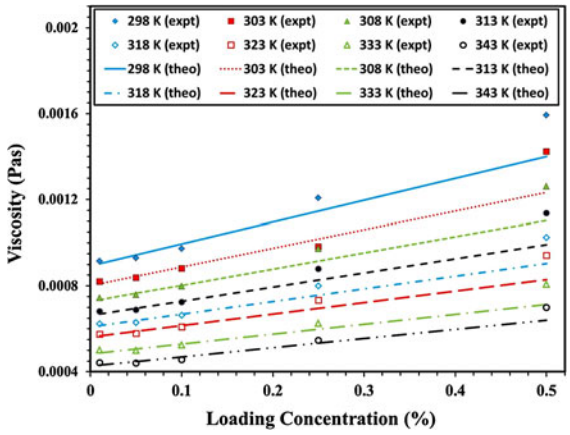

Fig. 6 Validation of analytic models for CNTS with experimental data for different loading concentrations

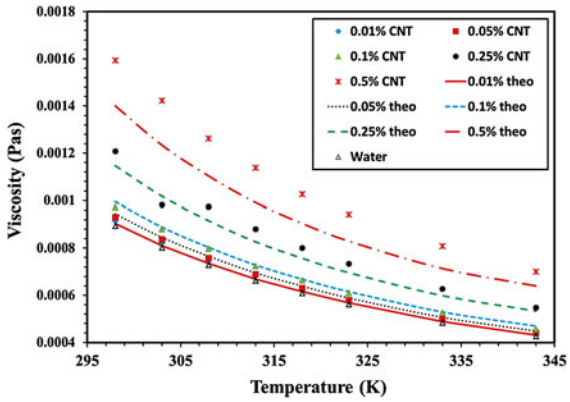

Fig. 7 Validation of analytic model for CNTS with experimental data for different temperatures

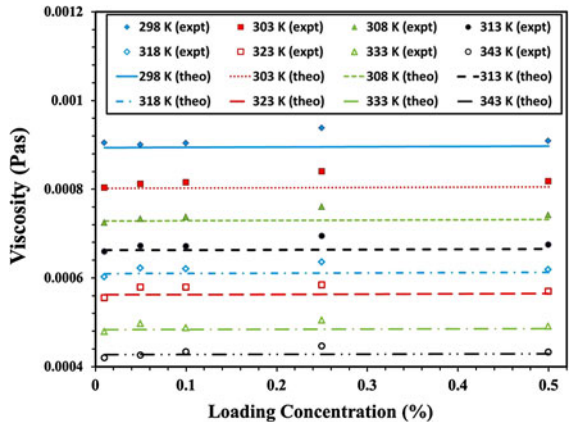

Fig. 8 Validation of analytic model for nAS with experimental data for different loading concentrations

In the case of a completely dynamic system, i.e., nAS, "α" is zero. In such cases, the composite model collapses to simply the viscosity term rendered by particle dynamics, and the plot for viscosity versus temperature and concentration has been provided in Fig. 8. In the case of nASs, the value of "$L\theta$" is determined to be one third that of the "$L\theta$" for graphene–water. The values for "a" and "b" are determined to be 15 and 4,530, respectively (for $T \geq 303$ K), and 0.4 and 109, respectively (for $T < 303$ K).

Conclusion

The viscosity of dilute GNSs has been experimentally determined, and their responses to temperature and concentration have been studied. Similar experimental studies have been carried out with CNTSs and nASs to understand the type of response exhibited by viscosity of nanofluids containing different categories of dispersed media. Viscosity response of graphene (with its sheet like structure) suspensions were seen to behave midway between those of CNT (cylindrical geometry) and alumina (spherical particles) suspensions. A mechanism based on this hybrid behavior and the CSS has been proposed to explain the viscous behavior of GNSs. It has been suggested from a comparison of CNTS, GNS, and nAS that sheet

percolation networks induce higher viscosity to suspensions than dynamic particles. Viscosity of suspensions has been explained based on the shear and disturbance induced within the fluid due to interparticle and particle–fluid molecule interactions. The mechanism of viscosity induced by percolation networks (formed by micron scale sheets) has been hypothesized to be the temperature-induced reshuffling and redistribution of individual sheets within the networks alongside adhesion–cohesion interplay-induced perturbations. In the case of the dynamic nanosheets, it has been suggested that they behave analogous to gas molecules within the base fluid matrix. However, their contribution to particle-induced viscosity is comparatively very little for percolation networks. The composite model for GNS viscosity has been found to be consistent and in agreement with experimental results within dilute limits. Similar consistence and agreeability have been observed in the case of completely static (CNTSs) and dynamic (nASs) systems too.

In conclusion, the present study throws light into the possible mechanism of solute-induced viscosity in graphene suspensions and the viscous response to temperature and concentration. As technologies, where GNSs might act as the starting material, such as graphene thin films, graphene-printed electronics, graphene bionanofluid-mediated drug delivery, etc., emerge into the forefront, the importance to understand the physics behind viscosity increases, since the suitability of the base fluid for such technologies is dependent on the viscous behavior of the nanofluid. It is evident from the present study that research into newer methods to control graphene sheet sizes during preparation in liquid medium will lead to economic and precise control over GNS viscosity and the consequential applications.

Acknowledgments The authors thank the Defense Materials and Stores Research & Development Establishment (DMSRDE) (a Defense Research and Development Organization (DRDO) laboratory) for financial support.

References

Anoop KB, Kabelac S, Sundararajan T, Das SK (2009) Rheological and flow characteristics of nanofluids: influence of electro-viscous effects and particle agglomeration. J App Phys 106:034909

Avsec J, Oblak M (2007) The calculation of thermal conductivity, viscosity and thermodynamic properties for nanofluids on the basis of statistical nanomechanics. Int J Heat Mass Trans 50:4331–4341

Bachelor GK (1977) The effect of Brownian motion on the bulk stress in a suspension of spherical particles. J Fluid Mech 83:97–117

Banerjee N, Koster G, Rijnders G (2013) Submicron patterning of epitaxial $PbZr_{0.52}Ti_{0.48}O_3$ heterostructures. Appl Phys Lett 102:142909

Chandrasekar M, Suresh S, Bose AC (2010) Experimental investigations and theoretical determination of thermal conductivity and viscosity of Al_2O_3/water nanofluids. Exp Thermal Fluids Sci 34:210–216

de Bruijin H (1942) The viscosity of suspensions of spherical particles. Recueil des trvaux chimiques des Pays-Bas 61:863–874

Dhar P, Gupta SS, Chakraborty S, Pattamatta A, Das SK (2013) Role of percolation and sheet dynamics during heat conduction in graphene nanofluids. Appl Phys Lett 102:163114

Dreyer DR, Park S, Bielawski CW, Ruoff RS (2010) The chemistry of graphene oxide. Chem Soc Rev 39:228

Eilers AM, Die HV (1941) Viskosititat von Emulsionen hochviskoser Stoffe Funktion der Konzentration. Kolloid Zeitschrift 97:313–321

Einstein A (1906) Eine neue Bestimmung der Moleküldimensionen. Annalen der Physik 19:289–306

Geim AK, Novoselov KS (2007) The rise of graphene. Nat Mater 6:183–191

Graham AL (1981) On the viscosity of suspensions of solid spheres. Appl Sci Res 37:275–286

Gupta SS, Siva VM, Krishnan S, Sreeprasad TS, Singh PK, Pradeep T, Das SK (2011) Thermal conductivity enhancement of nanofluids containing graphene nanosheets. J App Phys 110:084302

He Y, Jin Y, Chen H, Ding Y, Cang D, Lu H (2007) Heat transfer and flow behaviour of aqueous suspensions of TiO_2 nanoparticles (nanofluids) flowing upward through a vertical pipe. Int J Heat Mass Trans 50:2272–2281

Kole M, Dey TK (2010) Thermal conductivity and viscosity of Al_2O_3 nanofluid based on car engine coolant. J Phys D Appl Phys 43:315501

Krieger IM, Dougherty TJ (1959) A mechanism for non-Newtonian flow in suspensions of rigid spheres. Trans Soc Rheol 3:137–152

Kulkarni DP, Das DK, Chukwi GA (2006) Temperature dependent rheological property of CuO nanoparticles suspension. J Nanosci Nanotech 2006(6):1150–1154

Kurra N, Bhadram VS, Narayana C, Kulkarni GU (2013) Few layer graphene to graphitic films: infrared photoconductive *versus* bolometric response. Nanoscale 5:381–389

Li D, Muller MB, Gilje S, Kaner RB, Wallace GG (2008) Processable aqueous dispersions of graphene nanosheets. Nat Nanotechnol 3:101

Masoumi N, Sohrabi N, Behzadmehr A (2009) A new model for calculating the effective viscosity of nanofluids. J Appl Phys D 42:055501

Murshed SMS, Leong KC, Yang C (2008) Investigations of thermal conductivity and viscosity of nanofluids. Int J Therm Sci 47:560–568

Namburu PK, Kulkarni DP, Misra D, Das DK (2007) Viscosity of copper oxide nanoparticles dispersed in ethylene glycol and water mixture. Exp Therm Fluid Sci 32:397–402

Nguyen CT, Desgranges F, Roy G, Galanis N, Mare T, Boucher S, Mintsa HA (2007) Temperature and particle size dependent viscosity data for water based nanofluids–hysteresis phenomenon. Int J Heat Fluid Flow 28:1492–1506

Pak BC, Cho YI (1998) Hydrodynamic and heat transfer study of dispersed fluids with submicron metallic oxide particles. Exp Heat Trans 11:151–170

Phuoc TX, Massoudi M, Chen RH (2011) Viscosity and thermal conductivity of nanofluids containing multi-walled carbon nanotubes stabilized by chitosan. Int J Therm Sci 50:12–18

Prasher R, Song D, Wang J, Phelan P (2006) Measurements of nanofluid viscosity and its implications for thermal applications. Appl Phys Lett 89:133108

Sethi S, Ge L, Ci L, Ajayan PM, Dhinojwala A (2008) Gecko-inspired carbon nanotube-based self-cleaning adhesives. Nano Lett 8(3):822–825

Tseng WJ, Lin KC (2000) Rheology and colloidal structure of aqueous TiO_2 nanoparticle suspensions. Mat Sci Eng 355:186–192

Wang XQ, Mujumdar AS (2007) Heat transfer characters of nanofluids: a review. Int J Therm Sci 46:1–19